

Sheets of Spectral Data of Stokes Waves in Weakly Nonlinear Models

Benjamin Akers^{1*} and Ryan Creedon^{2†}

^{1*}Department of Mathematics and Statistics, Air Force Institute of Technology, 2950 Hobson Way, Wright Patterson AFB, 45433, OH, USA.

^{2†}Department of Applied Mathematics, Brown University, 75 Waterman St., Providence, 02912, RI, USA.

*Corresponding author(s). E-mail(s): benjamin.akers@afit.edu;

Contributing authors: ryan_creedon@brown.edu;

†These authors contributed equally to this work.

Abstract

We study the spectral stability of small-amplitude Stokes waves in a family of weakly nonlinear, unidirectional models of the form $\mathbf{u}_t + \mathbf{L}\mathbf{u} + (\mathbf{u}^2)_x = \mathbf{0}$. We introduce a perturbation method to expand the spectral data in wave amplitude near flat-state eigenvalue collisions, with the ratio of the colliding modes as a free parameter. This yields sheets of spectral data whose slices at fixed amplitude give isolas of instability. The same perturbation framework treats both high-frequency and Benjamin–Feir instabilities, extends to discontinuous dispersion relations (including the Akers–Milewski equation), and, for the first time, provides an analytic approximation of the Benjamin–Feir spectrum for this model and a direct comparison of high-frequency and Benjamin–Feir growth rates across the full family of models. Asymptotic predictions are validated against numerical spectra computed by Floquet–Fourier–Hill and quasi-Newton methods.

Keywords: Stokes waves, Benjamin-Feir instability, high-frequency instabilities, perturbation methods, resonant interactions

1 Introduction

Periodic traveling water waves have been studied for almost two centuries, beginning with the work of George Stokes. Provided the amplitude ε of these waves is sufficiently

Model	$\omega(k)$
Kawahara	$ak^3 + bk^5$
Whitham	$k\sqrt{\frac{\tanh(kh)}{k}}$
Capillary-Whitham	$k\sqrt{(1 + \sigma k^2)\frac{\tanh(kh)}{k}}$
Akers–Milewski	$\text{sgn}(k)(1 + \sigma k)^2$

Table 1 Example dispersion relations of weakly nonlinear models given by equation (1).

small, Stokes showed that these waves can be constructed as a power series in ε . For this reason, we refer to these waves as *Stokes waves*. A complete historical account of Stokes waves is given in [1].

The stability of Stokes waves has been investigated with both multi-scale and direct spectral methods. Beginning in the 1960s, multi-scale expansions led to amplitude equations such as the nonlinear Schrödinger, Dysthe, and Davey–Stewartson equations, in which the stability of Stokes waves to modulational sideband perturbations was analyzed in [2–8]. For more general perturbations, one obtains a spectral problem for the linearization of the governing water-wave equations about a Stokes wave. The spectra λ are purely continuous and parameterized by a Floquet exponent $p \in [0, 1)$, encoding the quasi-periodicity of the perturbations [9]. In the recent studies [10–14], asymptotic expansions of the unstable spectra and their corresponding Floquet exponents were obtained for sufficiently small ε , revealing various instabilities of Stokes waves, including the classic *modulational (or Benjamin–Feir) instability* as well as the newly discovered *high-frequency instabilities*.

In this work, we consider these asymptotic spectral expansions in the setting of a general family of weakly nonlinear models of the form

$$u_t + Lu + (u^2)_x = 0, \quad (1)$$

where L is a Fourier multiplier with purely imaginary symbol $\hat{L} = i\omega(k)$ and ω is the linear dispersion relation of the model. Equations of the form (1) are standard unidirectional models for surface water waves and related dispersive systems. Concrete examples include the Whitham, capillary–Whitham, Kawahara, and Akers–Milewski equations, whose dispersion relations we summarize in Table 1. For each such model, small-amplitude Stokes waves exist and are parametrically analytic in the amplitude ε [15, 16]. We investigate the unstable spectra of these waves for $0 < \varepsilon \ll 1$, noting that, since the specific models under consideration are weakly nonlinear approximations of the full water wave equations, the instability mechanisms we find have direct implications for water-wave dynamics.

Our first goal is to organize the spectral data near eigenvalue collisions of the linearization about the flat state. At zero amplitude ($\varepsilon = 0$), the stability spectrum

of (1) consists of imaginary eigenvalues $\lambda_0(k, p)$, indexed by the integer wavenumber $k \in \mathbb{Z}$ and Floquet exponent $p \in [0, 1)$. We consider (i) collisions of two nonzero eigenvalues at a Floquet exponent $p_0 \neq 0$, leading to high-frequency instabilities, and (ii) the collision of eigenvalues at the origin with $p_0 = 0$, corresponding to the Benjamin–Feir instability. For fixed $0 < \varepsilon \ll 1$, each collision of type (i) gives rise to a curve of unstable spectra parameterized by an ε -dependent interval of Floquet exponents p . This curve, known as an *isola of instability* in the water wave literature, is approximately an ellipse centered about the imaginary axis in the complex spectral plane. In contrast, for collision corresponding to the Benjamin–Feir instability, the curve is approximately a lemniscate centered at the origin.

To obtain asymptotic expansions for these curves of unstable spectra, one expands the eigenvalues, eigenfunctions, and Floquet exponent as power series in ε . As the calculations unfold, one realizes that a coefficient of the Floquet exponent expansion can be chosen as a free parameter, which ultimately parameterizes the curve of unstable spectra for fixed ε . Varying both ε and this parameter yields a 2D *sheet of spectral data* in $(\text{Re}\lambda, \text{Im}\lambda, \varepsilon)$ space.

Alternatively, one can choose the ratio β of the amplitudes of the colliding flat-state eigenfunctions to parameterize the curve of unstable eigenvalues for fixed ε . We opt for this choice for two reasons. First, the solvability conditions that appear at each order in the perturbation scheme reduce to linear systems, simplifying the algebra of the expansion while producing spectral data that agree with the previous parametrization after relabeling. Second, varying β naturally reveals important stability criterion like the classical Krein signature condition for high-frequency instabilities [17]. In fact, a trivial consequence of our calculations shows that this Krein condition is both necessary and sufficient for the onset of high-frequency instabilities in this class of models.

Building on earlier analyses of high-frequency and Benjamin–Feir instabilities in specific models [10–13], the present paper introduces three main novelties:

1. We develop a simple, direct perturbation method that produces both the high-frequency and Benjamin–Feir unstable spectra for the general model (1). The method yields not only the leading-order behavior of the unstable eigenvalues, but also their associated eigenfunctions and the most unstable growth rates. For high-frequency instabilities arising from type (i) collisions, we show that the structure of the resulting sheets of spectral data is organized by the resonant interaction between the carrier wave and the colliding modes: triad resonances ($|k_1 - k_2| = 1$) lead to elliptical isolas that are centred at the flat-state eigenvalue and have semi-major axes that scale as $\mathcal{O}(\varepsilon)$, while quartet resonances ($|k_1 - k_2| = 2$) produce elliptical isolas whose centres drift like $\mathcal{O}(\varepsilon^2)$ from the flat-state eigenvalue and have semi-major axes that scale as $\mathcal{O}(\varepsilon^2)$.
2. Because the same perturbation framework applies to both the high-frequency and Benjamin–Feir instabilities across a family of weakly nonlinear models, we can directly compare the magnitude of their growth rates for different choices of the dispersion relation. In particular, for representative models such as the Whitham, capillary–Whitham, Kawahara, and Akers–Milewski equations, we quantify how the

most unstable high-frequency eigenvalues compete with, or are dominated by, the Benjamin–Feir eigenvalues as the wave amplitude and wavenumber vary.

3. We formulate the Benjamin–Feir perturbation method so that it remains valid even when the dispersion relation is not differentiable. In particular, we successfully obtain the Benjamin–Feir unstable eigenvalues of the Akers–Milewski equation, whose dispersion relation has a jump discontinuity at $k = 0$ and therefore falls outside the smooth setting of [14] and related works. Our scheme only requires the pointwise values of $\omega(k)$ together with careful tracking of the singular terms that arise when ω has a jump. This allows us to obtain, to our knowledge, the first analytic approximation of the Benjamin–Feir spectrum for a model with discontinuous $\omega(k)$, and shows that the method we develop here is robust enough to treat equations with discontinuous dispersion, not just the classical smooth water-wave models.

Throughout, we compare the asymptotic predictions with numerical computations of the spectrum using two methods that are independent of the asymptotics: the Floquet–Fourier–Hill method [18] and a quasi-Newton continuation method for individual eigenpairs [19]. For representative choices of the dispersion relation—including the Whitham, capillary–Whitham, Kawahara, Boussinesq–Whitham, and Akers–Milewski equations—we find asymptotically correct agreement between the analytical and numerical spectra and highlight examples where higher-order terms play a significant quantitative role.

The paper is organized as follows. In Section 2, we formulate the general model, construct small-amplitude Stokes waves, and derive the associated spectral problem for general quasi-periodic perturbations parameterized by a Floquet exponent. In Section 3, we introduce the perturbation scheme for high-frequency instabilities near non-zero Floquet collisions and describe the resulting sheets and isolas of spectrum. In Section 4, we adapt the same framework to the Benjamin–Feir instability, derive the lemniscate approximating the figure-eight spectrum, and extend the method to the Akers–Milewski equation with discontinuous dispersion. We also compare directly the growth rates of the high-frequency and Benjamin–Feir instabilities across our family of models. Section 5 summarises our findings and outlines several directions for future work, including rigorous existence results for unstable spectra based on the bifurcation structure revealed here.

2 Stokes Waves and Spectral Stability Problem

2.1 Expansion of Stokes Waves

We seek periodic, traveling-wave solutions of (1) of the form

$$u(x, t) = u(\xi), \quad \xi = x - ct, \tag{2}$$

where c is the wave velocity. Without loss of generality, we restrict attention to 2π -periodic waves. Indeed, if one wishes to study a $2\pi/\kappa$ -periodic traveling wave of (1) for any $\kappa > 0$, one can rescale the traveling wave coordinate by

$$\xi \mapsto \kappa^{-1}\xi,$$

so that the wave becomes 2π -periodic. Under this rescaling, the dispersion relation and nonlinear term are modified in an elementary way, and κ appears as an additional parameter in the model. Thus it suffices to work with 2π -periodic waves, with the understanding that κ can be reintroduced when desired.

Substituting (2) into (1) yields the steady traveling-wave equation

$$-cu'(\xi) + Lu(\xi) + (u^2(\xi))' = 0, \quad (3)$$

where primes denote differentiation with respect to ξ . For the remainder of this manuscript, we replace ξ with x for ease of notation.

We are interested in small-amplitude solutions of (3) that bifurcate from a single Fourier mode. Let $\omega(k)$ denote the dispersion relation of (1) and $c_p(k) = \omega(k)/k$ the corresponding phase velocity. For definiteness, we take the carrier wavenumber to be $k = 1$ so that the linear wave has phase velocity

$$c_0 = c_p(1) = \omega(1).$$

Following standard constructions (see, for example, [15]), we introduce a small amplitude parameter $\varepsilon > 0$ and seek solutions of (3) of the form

$$u(x; \varepsilon) = \varepsilon \cos x + \varepsilon^2 u_2(x) + \varepsilon^3 u_3(x) + \dots, \quad c(\varepsilon) = c_0 + \varepsilon c_1 + \varepsilon^2 c_2 + \varepsilon^3 c_3 + \dots, \quad (4)$$

with 2π -periodic profiles u_j . Substituting (4) into (3) and equating powers of ε yields a hierarchy of linear problems for u_j , and solvability conditions of these linear problems determine the coefficients c_j . To second order in ε , one finds

$$u(x; \varepsilon) = \varepsilon \cos x + \varepsilon^2 \frac{1}{2(c_0 - c_p(2))} \cos(2x) + \mathcal{O}(\varepsilon^3), \quad (5a)$$

$$c(\varepsilon) = c_p(1) + \varepsilon^2 \frac{1}{2(c_0 - c_p(2))} + \mathcal{O}(\varepsilon^3), \quad (5b)$$

More generally, the Stokes expansion (4) can be continued to all orders in ε , and for each fixed dispersion relation $\omega(k)$ the resulting power series converge for sufficiently small ε ; see [15, 20] for rigorous results in this direction. In what follows, we regard ε as the primary bifurcation parameter for the family of Stokes waves and work with the expansion (5) as our model small-amplitude solution.

2.2 Stability Spectrum of Stokes Waves

To study the spectral stability of the Stokes wave $u(x; \varepsilon)$, we consider perturbations of the form

$$u(x, t) = u(x; \varepsilon) + v(x, t),$$

and linearize (1) about u . Writing $v(x, t)$ as a small perturbation and discarding quadratic and higher order terms in v yields the linearized equation

$$v_t - c(\varepsilon)v_x + Lv + 2(u(x; \varepsilon)v)_x = 0. \quad (6)$$

We seek normal modes of the form

$$v(x, t) = e^{\lambda t} v(x),$$

where $\lambda \in \mathbb{C}$ is the spectral parameter and $v(x)$ satisfies a Floquet (Bloch) boundary condition

$$v(x + 2\pi) = e^{2\pi i p} v(x), \quad p \in [0, 1), \quad (7)$$

with Floquet exponent p encoding the quasi-periodicity of the perturbation. Alternatively, we may write our normal mode as

$$v(x, t) = e^{\lambda t} e^{i p x} \tilde{v}(x), \quad (8)$$

such that $\tilde{v}(x)$ is a 2π -periodic function.

Substituting (8) into (6) and dropping the tilde on v for ease of notation, we arrive at the spectral stability problem

$$\lambda v - c(\varepsilon)(\partial_x + i p)v + \mathcal{L}v(x) + 2(\partial_x + i p)(u(x; \varepsilon)v(x)) = 0, \quad \text{where } \mathcal{L} := e^{-i p x} \circ L \circ e^{i p x}. \quad (9)$$

In Fourier space, the operator \mathcal{L} can be better seen as a multiplier with symbol

$$\hat{\mathcal{L}} = i\omega(k + p). \quad (10)$$

For each fixed $0 \leq \varepsilon \ll 1$ and $p \in [0, 1)$, the spectrum of (9) consists of a discrete set of eigenvalues $\lambda(p; \varepsilon)$ provided $v(x) \in L^2(0, 2\pi)$; see [9] for more details.

At zero amplitude ($\varepsilon = 0$), the Stokes wave reduces to the flat state $u \equiv 0$ and the wave velocity $c(\varepsilon)$ reduces to c_0 . In this limit, the spectral problem (9) simplifies to

$$\lambda v(x) - c_0 v_x(x) + \mathcal{L}v(x) = 0. \quad (11)$$

The eigenfunctions of (11) are the Fourier modes

$$v_{k,p}(x) = e^{i(k+p)x}, \quad k \in \mathbb{Z},$$

and the corresponding eigenvalues are

$$\lambda_0(k, p) = i(\omega(k + p) - c_0(k + p)), \quad k \in \mathbb{Z}, \quad p \in [0, 1). \quad (12)$$

The family $\{\lambda_0(k, p)\}_{k \in \mathbb{Z}, p \in [0, 1)}$ forms the Floquet–Bloch spectrum of the flat state, consisting entirely of imaginary eigenvalues.

As the amplitude ε of the Stokes wave is increased from zero, the spectrum of (9) deviates from the flat-state spectrum (12). Most importantly, bifurcations occur near repeated eigenvalues of (12). For nonzero repeated eigenvalues, we have (k_1, k_2, p_0) such that

$$\lambda_0(k_1, p_0) = \lambda_0(k_2, p_0) \neq 0,$$

for some Floquet exponent $p_0 \neq 0$ and integers $k_1 \neq k_2$. These eigenvalues give rise to the high-frequency instabilities when $0 < \varepsilon \ll 1$. In addition, we have a repeated

eigenvalue at $\lambda_0 = 0$ corresponding to the Benjamin–Feir instability. The perturbation schemes developed in the next two sections describe how these bifurcations unfold and generate the high-frequency and Benjamin–Feir instabilities summarized in the Introduction.

3 Asymptotics of High Frequency Instabilities

The unstable spectra approximated in this section are assumed to bifurcate from a flat-state ($\varepsilon = 0$), repeated eigenvalue given by $\lambda_0 = \lambda(k_1, p_0) = \lambda(k_2, p_0) \neq 0$ for some $p_0 \neq 0$ and $k_1 \neq k_2 \in \mathbb{Z}$. The corresponding eigenfunction can be written explicitly as

$$v_0 = \exp(i(k_1 + p_0)x) + \beta \exp(i(k_2 + p_0)x) = \phi_1(x) + \beta\phi_2(x). \quad (13)$$

Due to the repeated nature of λ_0 , the eigenfunction v_0 can be an arbitrary superposition of the modes ϕ_1 and ϕ_2 . In what follows, we normalize v_0 so that the coefficient of ϕ_1 is unity. The parameter β is also assumed to be nonzero. Otherwise, one finds that the higher-order corrections to the eigenvalues are imaginary and do not lead to instability.

We continue the eigenpair (λ_0, v_0) in ε by assuming the following power series expansions:

$$\lambda = \sum_{j=0}^{\infty} \lambda_j \varepsilon^j \quad \text{and} \quad v(\xi) = \sum_{j=0}^{\infty} v_j(\xi) \varepsilon^j, \quad (14)$$

where (λ, v) is an eigenpair of (9). We choose to normalize $v(\xi)$ so that $\langle v(\xi), \phi_1 \rangle = 1$, where $\langle \cdot, \cdot \rangle$ is the standard inner-product on $L^2(0, 2\pi)$:

$$\langle f, g \rangle = \frac{1}{2\pi} \int_0^{2\pi} \overline{f} g dx \quad \text{for} \quad f, g \in L^2(0, 2\pi). \quad (15)$$

Note that this choice of normalization implies $\langle v_0, \phi_1 \rangle = 1$, consistent with our normalization of v_0 , as well as implies $\langle v_j, \phi_1 \rangle = 0$ for all $j \geq 2$.

In addition to the expansions (14), we allow the Floquet exponent to vary analytically in ε :

$$p = \sum_{j=0}^{\infty} p_j \varepsilon^j, \quad (16)$$

as in [10–13]. By positing this expansion, we allow the interval of Floquet exponents parameterizing the unstable eigenvalues to vary with ε . Consequently, the operator \mathcal{L} becomes ε -dependent and requires the following expansion about $\varepsilon = 0$:

$$\hat{\mathcal{L}} = i\omega \left(k + \sum_{j=0}^{\infty} p_j \varepsilon^j \right)$$

$$\begin{aligned}
&= i\omega(k+p_0) + \varepsilon p_1 c_g(k+p_0) + \varepsilon^2 \left(p_2 c_g(k+p_0) + \frac{1}{2} p_1^2 c_g'(k+p_0) \right) + \mathcal{O}(\varepsilon^3), \\
&= \hat{\mathcal{L}}_0 + \varepsilon \hat{\mathcal{L}}_1 + \varepsilon^2 \hat{\mathcal{L}}_2 + \mathcal{O}(\varepsilon^3).
\end{aligned} \tag{17}$$

Here, $c_g(k) = \omega'(k)$ is the group velocity and primes denote differentiation in k . The $\mathcal{O}(\varepsilon)$ equation for the spectral data (λ, v) is

$$(\lambda_0 - c_0 \partial_\xi + \mathcal{L}_0) v_1 = -\lambda_1 v_0 + c_0 i p_1 v_0 - \mathcal{L}_1 v_0 - 2(v_0 u_1)_x. \tag{18}$$

From the choice of eigenpair (λ_0, v_0) , the modes ϕ_1 and ϕ_2 are in the nullspace of the operator $(\lambda_0 - c_0 \partial_x + \mathcal{L}_0)$. In order for (18) to admit a consistent solution for v_1 , the Fredholm alternative enforces two solvability conditions, namely

$$\langle \phi_j, -\lambda_1 v_0 + c_0 i p_1 v_0 - \mathcal{L}_1 v_0 - 2(v_0 u_1)_x \rangle = 0, \quad \text{for } j \in \{1, 2\}.$$

These conditions reduce to

$$\begin{pmatrix} -1 & -i\tilde{c}_g(k_1 + p_0) \\ -\beta & -i\tilde{c}_g(k_2 + p_0)\beta \end{pmatrix} \begin{pmatrix} \lambda_1 \\ p_1 \end{pmatrix} = \begin{pmatrix} \langle \phi_1, 2(v_0 u_1)_x \rangle \\ \langle \phi_2, 2(v_0 u_1)_x \rangle \end{pmatrix}, \tag{19}$$

where we have introduced the group velocity in the traveling frame $\tilde{c}_g(k) = c_g(k) - c_0$ to simplify the appearance of these conditions.

Remark 3.1. To compute the corrections to the flat-state spectral data, one needs two bifurcation parameters to satisfy the two solvability conditions that appear at $\mathcal{O}(\varepsilon)$ and at subsequent orders. In this work, corrections to the Floquet exponent p_j and the eigenvalue λ_j are chosen to satisfy the solvability conditions, while β is a free choice. By varying β , one obtains sheets of spectral data. This is in contrast to the approach of [10–13], where β is expanded as a power series in ε and its corrections, alongside the eigenvalue corrections, are the solvability parameters. The corrections to the Floquet exponent in that framework are free.

Remark 3.2. Regardless of the frequency difference in the eigenfunctions $k_2 - k_1$, one always solves a linear system for p_1 and λ_1 . This contrasts [10–13], where the solvability conditions are nonlinear. Moreover the matrix which must be inverted for these (and the later) solvability conditions has a clear nondegeneracy condition given by the determinant

$$\det \begin{pmatrix} -1 & -i\tilde{c}_g(k_1 + p_0) \\ -\beta & -i\tilde{c}_g(k_2 + p_0)\beta \end{pmatrix} = i\beta(\tilde{c}_g(k_2 + p_0) - \tilde{c}_g(k_1 + p_0)).$$

If $\tilde{c}_g(k_2 + p_0) - \tilde{c}_g(k_1 + p_0) \neq 0$ then the solution formally exists for all $\beta \neq 0$.

Remark 3.3. Equation (19) is forced by nonlinear interactions

$$\langle \phi_j, 2(v_0 u_1)_x \rangle = \frac{1}{2\pi} \int_0^{2\pi} e^{-i(k_j+p_0)x} \left((e^{ix} + e^{-ix})(e^{i(k_1+p_0)x} + \beta e^{i(k_2+p_0)x}) \right)_x dx. \quad (20)$$

For the above integrals to be nonzero, one needs a relationship between the wavenumbers of the eigenfunctions, k_1 and k_2 , and that of the carrier wave, $k = 1$. The relationship is a triad condition, $k_1 = k_2 \pm 1$, without which there is no instability at this order. Later orders will have a similar requirement, where the solvability conditions give rise to homogeneous linear equations unless the wavenumbers take part in a resonance interaction.

Before proceeding with our analysis of (19), we note that the repeated eigenvalue λ_0 implies a resonance between the wavenumbers of the eigenmodes k_j and that of the carrier wave $k = 1$, namely

$$\lambda(k_1, p_0) = \lambda(k_2, p_0) \implies ic_0(k_1 + p_0) - i\omega(k_1 + p_0) = ic_0(k_2 + p_0) - i\omega(k_2 + p_0).$$

Using $c_0 = c_p(1) = \omega(1)$ and defining $m = k_1 - k_2$, we can rewrite this resonance condition as

$$m - k_1 + k_2 = 0 \quad \text{and} \quad m\omega(1) - \omega(k_1 + p) + \omega(k_2 + p) = 0, \quad (21)$$

which represents a resonance between $|m| + 2$ waves. For $|m| > 1$, the resonance is degenerate because the wavenumber $k = 1$ is repeated $|m|$ times. In the language of resonant interaction theory [21, 22], the $|m| = 1$ resonance represents a triad interaction, the $|m| = 2$ resonance represents a quartet interaction, and the $|m| \geq 3$ resonances represent high-order interactions. As will be seen, each value of m gives rise to a different high-frequency instability as ε increases from zero. Therefore, it is natural for us to label high-frequency instabilities according to the value of m in (21) as triad ($|m| = 1$), quartet ($|m| = 2$), and higher-order ($|m| \geq 3$) high-frequency instabilities.

3.1 High Frequency Instabilities: Triads

In this subsection, we assume that the wavenumbers k_j of the flat-state eigenfunction take part in a triad resonance so that $|k_1 - k_2| = 1$. For notational convenience we will define k_2 to be the larger of the two wavenumbers so that $k_2 = k_1 + 1$. No generality is lost here: since β is already restricted to not be zero, swapping the roles of k_1 and k_2 can be accomplished by dividing v by β . Having chosen the triad resonance for k_1 and k_2 , the right hand side of equation (19) can be evaluated explicitly, yielding

$$\begin{pmatrix} -1 & -i\tilde{c}_g(k_1 + p_0) \\ -\beta & -i\tilde{c}_g(k_2 + p_0) \end{pmatrix} \begin{pmatrix} \lambda_1 \\ p_1 \end{pmatrix} = \begin{pmatrix} \beta i(k_1 + p_0) \\ i(k_2 + p_0) \end{pmatrix}, \quad (22)$$

whose solution is

$$\lambda_1 = \frac{i \{ \tilde{c}_g(k_1 + p_0)(k_2 + p_0) - \beta^2(k_1 + p_0)\tilde{c}_g(k_2 + p_0) \}}{\beta(\tilde{c}_g(k_2 + p_0) - \tilde{c}_g(k_1 + p_0))},$$

$$p_1 = \frac{\beta^2(k_1 + p_0) - (k_2 + p_0)}{\beta(\tilde{c}_g(k_2 + p_0) - \tilde{c}_g(k_1 + p_0))} = \frac{\beta(k_1 + p_0) - (k_2 + p_0)\beta^{-1}}{(\tilde{c}_g(k_2 + p_0) - \tilde{c}_g(k_1 + p_0))}.$$

The eigenvalue correction, λ_1 , is clearly imaginary for real β . However, since the eigenfunction v of this spectral problem can be complex-valued, β can be complex. In contrast, the Floquet exponent p must be real, so $p_1 \in \mathbb{R}$. Writing $\beta = \rho \exp(i\theta)$,

$$p_1 = \frac{\rho(\cos(\theta) + i \sin(\theta))(k_1 + p_0) - (k_2 + p_0)\rho^{-1}(\cos(\theta) - i \sin(\theta))}{(c_g(k_2 + p_0) - c_g(k_1 + p_0))}.$$

To have real p_1 , one requires

$$(\rho(k_1 + p_0) + (k_2 + p_0)\rho^{-1}) \sin(\theta) = 0.$$

Thus, either $\sin(\theta) = 0$ (and β is real) or $\rho^2 = \frac{-(k_2 + p_0)}{(k_1 + p_0)}$ has real solutions. Since $\beta \in \mathbb{R}$ gives a purely imaginary (and, hence, stable) eigenvalue correction and since ρ is real by definition, one needs

$$\frac{k_2 + p_0}{k_1 + p_0} = \frac{k_1 + 1 + p_0}{k_1 + p_0} < 0,$$

to achieve instability. The above condition is, in fact, a representation of the Krein signature computed in [11, 17], which is a necessary condition for the formation of high-frequency instabilities. As we have just shown, it is also a sufficient condition.

Without loss of generality, we choose $k_1 = -1$, $k_2 = 0$, and $\rho = \sqrt{\frac{p_0}{(1-p_0)}}$, giving us

$$p_1 = \left(\frac{\rho(k_1 + p_0) - (k_2 + p_0)\rho^{-1}}{(\tilde{c}_g(k_2 + p_0) - \tilde{c}_g(k_1 + p_0))} \right) \cos(\theta),$$

for any $\theta \in (0, 2\pi)$ and

$$\text{Im}(\lambda_1) = \frac{(-\rho(k_1 + p_0)\tilde{c}_g(k_2 + p_0) + \rho^{-1}\tilde{c}_g(k_1 + p_0))(k_2 + p_0)}{(\tilde{c}_g(k_2 + p_0) - \tilde{c}_g(k_1 + p_0))} \cos(\theta), \quad (23a)$$

$$\text{Re}(\lambda_1) = -\frac{(\rho(k_1 + p_0)\tilde{c}_g(k_2 + p_0) + \rho^{-1}\tilde{c}_g(k_1 + p_0))(k_2 + p_0)}{(\tilde{c}_g(k_2 + p_0) - \tilde{c}_g(k_1 + p_0))} \sin(\theta). \quad (23b)$$

Thus, λ_1 predicts an elliptical isola centered at λ_0 for any sufficiently small ε . This ellipse is parameterized by θ . Eigenvalues on this isola with positive real part are responsible for generating triad high-frequency instabilities. Example isolas for the deep water gravity-capillary Whitham equation and the Akers–Milewski equation are shown in Figure 1. When both ε and θ are varied, (23) predicts a sheet of spectral data arranged on a conical surface; see, for instance, Figure 2.

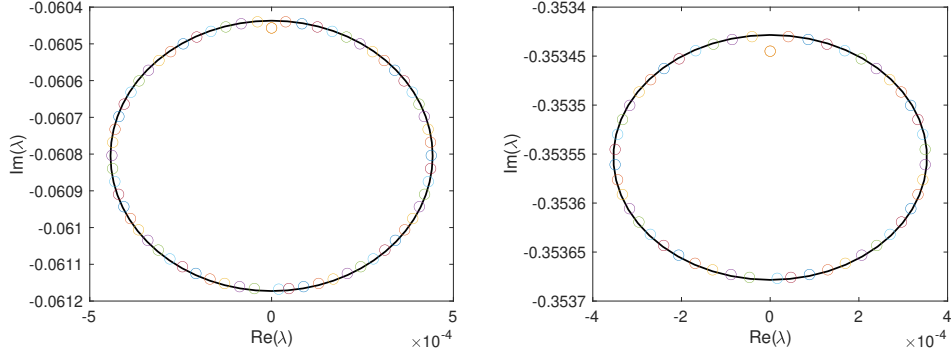


Fig. 1 *Left:* An isola of a triad instability in the deep water ($h \rightarrow \infty$) gravity-capillary Whitham equation near $(\lambda_0, p_0) \approx (-0.0608i, 0.2681)$ with $\sigma = 2.5$ at $\varepsilon = 10^{-3}$. The circles are computed with a quasi-Newton iteration; the curves are the asymptotic prediction of (23). *Right:* An isola of a triad instability in the Akers-Milewski equation near $(\lambda_0, p_0) = (0.3536i, 0.1464)$ with $\sigma = 2$ at $\varepsilon = 10^{-3}$. The circles are computed with a quasi-Newton iteration; the curves are the asymptotic prediction of (23).

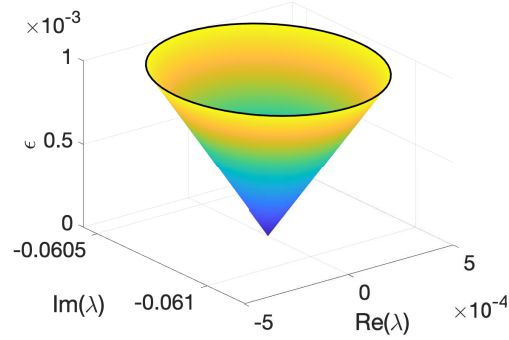


Fig. 2 The surface of spectral data predicted by (23) in the deep water ($h \rightarrow \infty$) gravity-capillary Whitham equation is visualized. The spectrum bifurcated from $(\lambda_0, p_0) \approx (-0.0608i, 0.2681)$ with $\sigma = 2.5$. This is the same configuration which is compared to numerical predictions in Figure 1.

3.1.1 High Frequency Instabilities: Quartets

If the wavenumber difference is larger than one, $|k_1 - k_2| > 1$, then the integrals in (20) vanish, and the corrections p_1 and λ_1 are zero. Thus, there is no instability at $\mathcal{O}(\varepsilon)$. Equation (18) can be readily solved for v_1 , giving us

$$v_1 = \alpha_1^- e^{i(k_1+p_0-1)x} + \alpha_1^+ e^{i(k_1+p_0+1)x} + \beta\alpha_2^- e^{i(k_2+p_0-1)x} + \beta\alpha_2^+ e^{i(k_2+p_0+1)x},$$

where $\alpha_j^\pm = \frac{-i(k_j+p_0\pm 1)}{\lambda_0(k_j+p_0) - \lambda_0(k_j+p_0\pm 1)}$ are real coefficients.

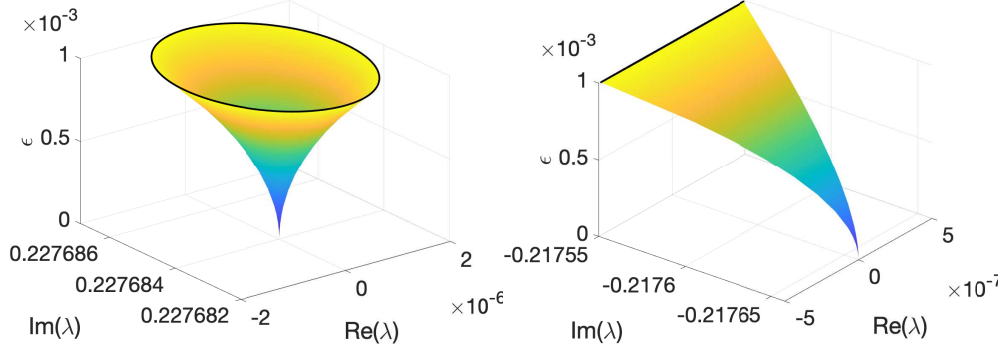


Fig. 3 *Left:* The surface of spectral data predicted by (27) in the Kawahara equation is visualized. The spectrum bifurcates from $(\lambda_0, p_0) \approx (0.2277i, 0.3675)$ with $(a, b) = (1, -0.25)$. This is the same configuration which is compared to numerical predictions in Figure 4. *Right* The surface of spectral data predicted by (27) in the deep water gravity-capillary Whitham equation is visualized. The spectrum bifurcates from $(\lambda_0, p_0) \approx (0.2177i, 0.1363)$ with $\sigma = 0.25$. This is the same configuration which is compared to numerical predictions in Figure 5.

At $\mathcal{O}(\varepsilon^2)$, the spectral problem (9) becomes

$$(\lambda_0 - c_0 \partial_x + \mathcal{L}_0)v_2 = -\lambda_2 v_0 + c_2 v_{0,x} + c_0 i p_2 v_0 - \mathcal{L}_1 v_1 - \mathcal{L}_2 v_0 - 2(v_1 u_1 + v_0 u_2)_x, \quad (24)$$

where \mathcal{L}_1 and \mathcal{L}_2 are Fourier multipliers with symbols defined in (17). Following the same calculations for the solvability conditions as in the $\mathcal{O}(\varepsilon)$ problem, one arrives at

$$\begin{pmatrix} -1 & -i\tilde{c}_g(k_1 + p_0) \\ -\beta & -i\tilde{c}_g(k_2 + p_0)\beta \end{pmatrix} \begin{pmatrix} \lambda_2 \\ p_2 \end{pmatrix} = \begin{pmatrix} \langle \phi_1, 2(v_0 u_2 + v_1 u_1)_x \rangle - c_2 i(k_1 + p_0) \\ \langle \phi_2, 2(v_0 u_2 + v_1 u_1)_x \rangle - c_2 i(k_2 + p_0)\beta \end{pmatrix} \quad (25)$$

The coefficient matrix above is identical to the triad setting and invertible whenever $\beta \neq 0$ and $\tilde{c}_g(k_1 + p_0) \neq \tilde{c}_g(k_2 + p_0)$. The right-hand side represents new possible resonances between k_1 and k_2 .

3.1.2 Quartet Resonances

Consider a quartet resonance between k_2 and k_1 for $k_2 > k_1$ without loss of generality. Then, $k_2 = k_1 + 2$, and the solvability conditions (25) simplify to

$$\begin{pmatrix} -1 & -i\tilde{c}_g(k_1 + p_0) \\ -\beta & -i\tilde{c}_g(k_2 + p_0)\beta \end{pmatrix} \begin{pmatrix} \lambda_2 \\ p_2 \end{pmatrix} = \begin{pmatrix} i(k_1 + p_0) \{ \alpha_1^+ + \alpha_1^- - c_2 + (\alpha_2^- + D)\beta \} \\ i(k_2 + p_0) \{ (\alpha_2^+ + \alpha_2^- - c_2)\beta + (\alpha_1^+ + D) \} \end{pmatrix}, \quad (26)$$

with solutions

$$\lambda_2 = i \frac{A\beta^2 + B\beta + C}{\beta} \quad \text{and} \quad p_2 = \frac{E\beta^2 + F\beta + G}{\beta}.$$

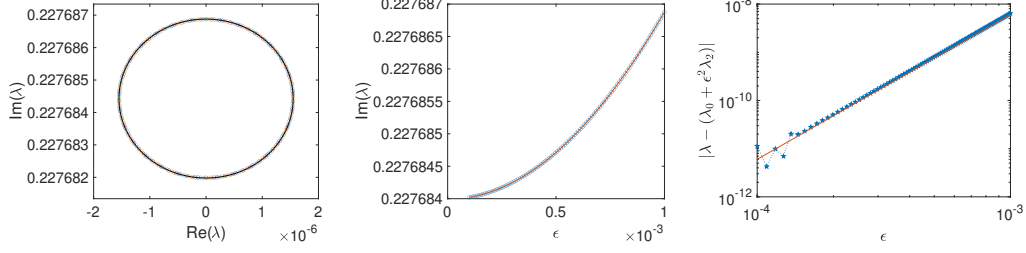


Fig. 4 *Left:* An isola of a quartet instability in the Kawahara equation near $(\lambda_0, p_0) = (0.2277i, 0.3675)$ with $(a, b) = (1, -0.25)$ at $\varepsilon = 10^{-3}$. The circles are computed with a quasi-Newton iteration; the curves are the second order asymptotic prediction of (27). *Center:* The imaginary part of the most unstable eigenvalue of (27) (solid line) against numerical computations from a quasi-Newton iteration (circles). *Right:* The error between the numerically computed and asymptotics (27) (starred line); the solid line marks $y = 6\varepsilon^3$.

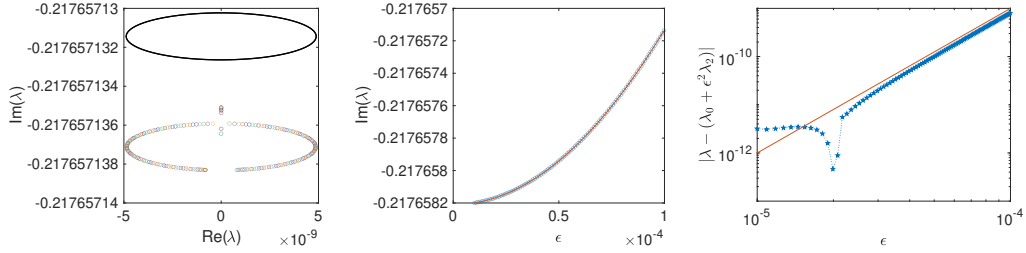


Fig. 5 *Left:* An isola of a quartet instability in the deep-water gravity-capillary Whitham equation near $(\lambda_0, p_0) = (0.2177i, 0.1363)$ with $\sigma = 0.25$ at $\varepsilon = 10^{-4}$. The circles are computed with a quasi-Newton iteration; the curves are the second order asymptotic prediction of (27). *Center:* The imaginary part of the most unstable eigenvalue of (27) (solid line) against numerical computations from a quasi-Newton iteration (circles). *Right:* The error between the numerically computed and asymptotics (27) (starred line); the solid line marks $y = 10^3 \varepsilon^3$.

Here, A, B, C, E, F , and G are real-valued coefficients given by

$$\begin{aligned}
 A &= \frac{-\tilde{c}_g(k_2 + p_0)(k_1 + p_0)(\alpha_2^- + D)}{\tilde{c}_g(k_2 + p_0) - \tilde{c}_g(k_1)}, \\
 B &= \frac{-\tilde{c}_g(k_2 + p_0)(k_1 + p_0)(\alpha_1^+ + \alpha_1^- - c_2) + \tilde{c}_g(k_1 + p_0)(k_2 + p_0)(\alpha_2^+ + \alpha_2^- - c_2)}{\tilde{c}_g(k_2 + p_0) - \tilde{c}_g(k_1 + p_0)}, \\
 C &= -\frac{-\tilde{c}_g(k_1 + p_0)(k_2 + p_0)(\alpha_1^+ + D)}{\tilde{c}_g(k_2 + p_0) - \tilde{c}_g(k_1 + p_0)}, \\
 E &= \frac{(k_1 + p_0)(\alpha_2^- + D)}{\tilde{c}_g(k_2 + p_0) - \tilde{c}_g(k_1 + p_0)}, \\
 F &= \frac{(k_1 + p_0)(\alpha_1^+ + \alpha_1^- - c_2) - (k_2 + p_0)(\alpha_2^+ + \alpha_2^- - c_2)}{\tilde{c}_g(k_2 + p_0) - \tilde{c}_g(k_1 + p_0)}, \\
 G &= -\frac{(k_2 + p_0)(\alpha_1^+ + D)}{\tilde{c}_g(k_2 + p_0) - \tilde{c}_g(k_1 + p_0)}.
 \end{aligned}$$

If $\beta \in \mathbb{R}$, then λ_2 is imaginary, similar to what occurs for λ_1 in the triad case. If β is complex, then $\beta = \rho e^{i\theta}$ and

$$p_2 = E\rho e^{i\theta} + F + G\rho^{-1}e^{-i\theta}.$$

It follows that

$$\text{Im}(p_2) = E\rho \sin(\theta) - G\rho^{-1} \sin(\theta).$$

To ensure the Floquet exponent remains real-valued, we must enforce either $\sin(\theta) = 0$ (leading to $\beta \in \mathbb{R}$) or, more interestingly, $\rho^2 = \frac{G}{E}$ and θ is free. For quartet high-frequency instabilities to occur, we must have $G/E > 0$. As in the triad case, this sign condition is exactly the Krein signature of the repeated eigenvalue λ_0 . Our work shows that this Krein condition is necessary and sufficient to develop quartet high-frequency instabilities.

Given the choice of β above and assuming the Krein condition holds, the formula for the eigenvalue corrections is

$$\lambda_2 = i \left(A\sqrt{\frac{G}{E}}(\cos(\theta) + i \sin(\theta)) + B + C\sqrt{\frac{E}{G}}(\cos(\theta) - i \sin(\theta)) \right), \quad (27)$$

which has real and imaginary parts given by

$$\text{Re}(\lambda_2) = \left(-A\sqrt{\frac{G}{E}} + C\sqrt{\frac{E}{G}} \right) \sin(\theta), \quad (28a)$$

$$\text{Im}(\lambda_2) = \left(A\sqrt{\frac{G}{E}} + C\sqrt{\frac{E}{G}} \right) \cos(\theta) + B. \quad (28b)$$

respectively. From these expressions, we see that quartet high-frequency instabilities also appear as ellipses in the complex spectral plane. However, unlike the triad case, these ellipses have semi-major axes that scale as $\mathcal{O}(\varepsilon^2)$, and their centers drift along the imaginary axis at a distance from λ_0 that grows like $\mathcal{O}(\varepsilon^2)$.

An example of a quartet high-frequency instability for the Kawahara equation appears in Figure 4, along with three different evaluations that demonstrate the validity of our asymptotic calculations. The left panel compares the shape and location of the asymptotic prediction of the isola (varying θ with fixed ε) to numerical computations of the spectrum computed with a quasi-Newton iteration. The center panel compares plots of the imaginary component of the most unstable eigenvalue as a function of ε according to (27) and to numerical computations. The right panel shows a log-log plot of the difference between the asymptotic and numerical predictions of the most unstable eigenvalue as a function of ε . From this log-log plot, we see that the observed errors are $\mathcal{O}(\varepsilon^3)$, as expected. When $\varepsilon = 10^{-3}$, errors are less than 10^{-8} , hence the clear visible match between the asymptotic and numerical predictions in the left and center panel.

A quartet high-frequency instability isola for the deep water gravity-capillary Whitham equation appears in Figure 5, along with similar evaluations supporting the

validity of our calculations. Unlike the Kawahara equation, the numerics and asymptotics appear to disagree about the center of the isola. In the right panel of Figure 5, a log-log plot of the difference between numerics and asymptotics shows that these errors have leading-order behavior $q \cdot \varepsilon^3$ for $q \approx 10^3$. That the exponent of this behavior is three gives confidence that our asymptotic calculations are correct. However, the prefactor q is quite large. As a consequence, we conclude that the cubic eigenvalue corrections of the Whitham equation are much larger than they were in the Kawahara example. This suggests that, if one were to compute the entire series, as in [23], the spectrum near this collision may have a small radius of convergence.

3.1.3 Higher-Order Resonances

If $|k_1 - k_2| > 2$, the solvability conditions simplify to

$$\begin{pmatrix} -1 & -i\tilde{c}_g(k_1 + p_0) \\ -\beta & -i\tilde{c}_g(k_2 + p_0)\beta \end{pmatrix} \begin{pmatrix} \lambda_2 \\ p_2 \end{pmatrix} = \begin{pmatrix} i(k_1 + p_0)(\alpha_1^+ + \alpha_1^- - c_2) \\ i(k_2 + p_0)(\alpha_2^+ + \alpha_2^- - c_2)\beta \end{pmatrix}. \quad (29)$$

Note that β appears in the second component of the right-hand side vector, as opposed to the first component when $|k_1 - k_2| = 2$. Assuming $\beta \neq 0$, we can divide β from the second solvability condition, leaving behind solutions for λ_2 and p_2 that are independent of β :

$$\lambda_2 = \frac{i \{ -(k_1 + p_0)\tilde{c}_g(k_2 + p_0)(\alpha_1^+ + \alpha_1^- - c_2) + \tilde{c}_g(k_1 + p_0)(k_2 + p_0)(\alpha_2^+ + \alpha_2^- - c_2) \}}{\tilde{c}_g(k_2 + p_0) - \tilde{c}_g(k_1 + p_0)},$$

$$p_2 = \frac{(k_1 + p_0)(\alpha_1^+ + \alpha_1^- - c_2) - (k_2 + p_0)(\alpha_2^- + \alpha_2^+ - c_2)}{\tilde{c}_g(k_2 + p_0) - \tilde{c}_g(k_1 + p_0)}$$

Since $\alpha_{j,\pm} \in \mathbb{R}$, we must have $\lambda_2 \in i\mathbb{R}$ and $p_2 \in \mathbb{R}$ for all $\beta \neq 0$. Thus, higher-order resonances do not lead to instability at $\mathcal{O}(\varepsilon^2)$. In fact, one would expect that the m th resonant high-frequency instability has the first opportunity to generate instability at $\mathcal{O}(\varepsilon^m)$. This is precisely what occurs in the finite-depth water wave problem.

4 The Benjamin-Feir Instability

Unstable eigenvalues of the Benjamin-Feir instability bifurcate from the zero eigenvalue of the flat-state spectrum. A direct calculation shows this eigenvalue has corresponding Floquet exponent $p_0 = 0$ and the wavenumbers k in its eigenspace satisfy the resonance condition

$$\lambda_0 = ic_0k - i\omega(k) = 0,$$

where $c_0 = \omega(1)$. If we assume

- (i) $\omega(k)$ is odd,

- (ii) $\inf_{k \in \mathbb{N}_0 \setminus \{1\}} |\omega(k)/k - \omega(1)| > 0$, and
- (iii) $\omega(k)/k \in \mathcal{C}^\alpha(\mathbb{R})$ for $\alpha \geq 3$,

as in [20], then the only solutions of the resonance condition are $k_1 = -1$, $k_2 = 0$, and $k_3 = 1$. Hence, $\lambda_0 = 0$ has geometric multiplicity three with eigenspace

$$v_0 = \beta_{0,-1} \exp(-ix) + \beta_{0,0} + \beta_{0,1} \exp(ix),$$

for $\beta_{0,0}$ and $\beta_{0,\pm 1} \in \mathbb{C}$.

To capture unstable eigenvalues when $0 < \varepsilon \ll 1$, we expand the spectral data (λ, v) of (9) as power series in ε , much like the high-frequency instabilities. However, to ease the burden of the calculations that follow, we will re-express the spectral problem in the form

$$Tv = \lambda v, \quad \text{where} \tag{30}$$

$$T := i \left(c(p+D)v - \omega(p+D)v - 2(p+D)(uv) \right) \quad \text{and} \quad D = -i\partial_x.$$

We normalize the eigenfunction v according to

$$\int_{-\pi}^{\pi} v e^{ix} dx = 1,$$

so that $\beta_{0,-1} = 1$ and all subsequent corrections of v exclude the $\exp(-ix)$ mode.

In addition to the spectral data, we expand the Floquet exponent p in terms of a renormalized series

$$p = \varepsilon p_1 (1 + r(\varepsilon)), \quad \text{with} \quad r(\varepsilon) = \sum_{n=1}^{\infty} r_n \varepsilon^n.$$

As will be seen, p_1 belongs to a real-valued interval that is symmetric about zero, while $r(\varepsilon)$ rescales the radius of this interval as ε increases. For the triad and quartet instabilities of the previous sections, the interval of p corresponding to the unstable eigenvalues can have a non-zero midpoint. Thus, a traditional power series expansion is appropriate to capture these instabilities. In contrast, the interval of p parameterizing the unstable eigenvalues of the Benjamin-Feir instability is always symmetric about zero. The renormalized expansion above reflects this additional constraint. For more details, see [14].

In light of (iii), we define the operators

$$T_n := \frac{1}{n!} \frac{d^n T}{d\varepsilon^n} \Big|_{\varepsilon=0}, \quad \text{for} \quad n \in \{0, \dots, \alpha\}.$$

It follows that the $\mathcal{O}(\varepsilon)$ terms of (30) take the form

$$T_0 v_1 = (\lambda_1 - T_1) v_0, \tag{31}$$

yielding an inhomogeneous linear equation for v_1 . To ensure the solvability of (31), the Fredholm alternative requires that the inhomogeneous terms are orthogonal to the nullspace of the adjoint of T_0 . Since T_0 is skew self-adjoint, we can instead enforce orthogonality between the inhomogeneous terms and v_0 , leading to the following solvability conditions:

$$\lambda_1 + i\tilde{c}_g(-1)p_1 - i\beta_{0,0} = 0, \quad (32a)$$

$$\left(\lambda_1 + i\tilde{c}_g(0)p_1\right)\beta_{0,0} = 0, \quad (32b)$$

$$\left(\lambda_1 + i\tilde{c}_g(1)p_1\right)\beta_{0,1} + i\beta_{0,0} = 0. \quad (32c)$$

To simplify the appearance of these conditions, we continue to use $\tilde{c}_g(k) := \omega'(k) - c_0$ as the linear group velocity of (1) in a frame traveling at velocity c_0 . Note by (i) that $\tilde{c}_g(-k) = \tilde{c}_g(k)$ for all $k \in \mathbb{R}$.

System (32a)-(32c) admits many possible solutions, all of which imply that λ_1 is imaginary and, hence, no instability is observed at $\mathcal{O}(\varepsilon)$. Hindsight shows that there is a unique solution of these conditions that leads to eigenvalues with positive real part at $\mathcal{O}(\varepsilon^2)$. In particular, one should choose $\lambda_1 = -i\tilde{c}_g(1)p_1$ and $\beta_{0,0} = 0$, while p_1 and $\beta_{0,1}$ remain arbitrary at this order.

Having solved (32a)-(32c), we return to (31), invert T_0 against its range, and solve for v_1 . Upon doing so, we find

$$v_1 = v_{1,-2} \exp(-2ix) + v_{1,2} \exp(2ix) + \beta_{1,0} + \beta_{1,1} \exp(ix),$$

where $\beta_{1,0}, \beta_{1,1} \in \mathbb{C}$,

$$v_{1,-2} = \frac{1}{c_0 - \frac{\omega(2)}{2}}, \quad \text{and} \quad v_{1,2} = \frac{\beta_{0,1}}{c_0 - \frac{\omega(2)}{2}}. \quad (33)$$

Note that $v_{1,\pm 2}$ are well-defined by (ii).

At $\mathcal{O}(\varepsilon^2)$, (30) becomes

$$T_0 v_2 = (\lambda_1 - T_1)v_1 + (\lambda_2 - T_2)v_0.$$

Like the previous order, we require the inhomogeneous terms to satisfy the Fredholm alternative, leading us (after some work) to the following solvability conditions:

$$\beta_{1,0} = \frac{1 + \beta_{0,1}}{\omega'(1) - \omega'(0)}, \quad (34a)$$

$$i\lambda_2 - \tilde{c}_g(1)r_1p_1 - (U + Vp_1^2) = U\beta_{0,1}, \quad (34b)$$

$$\beta_{0,1} \left(i\lambda_2 - \tilde{c}_g(1)r_1p_1 + U + Vp_1^2 \right) = -U, \quad (34c)$$

where

$$U = \frac{1}{\omega'(0) - \omega'(1)} + \frac{1}{\omega(2) - 2c_0} \quad \text{and} \quad V = -\frac{1}{2}\omega''(1). \quad (35)$$

By combining (34b) and (34c) to eliminate p_1^2 and then to eliminate λ_2 , respectively, we find

$$\lambda_2 = -i\tilde{c}_g(1)r_1p_1 + i\frac{U}{2} \cdot \frac{(1 - \beta_{0,1}^2)}{\beta_{0,1}}, \quad (36)$$

$$p_1^2 = -\frac{U}{2V} \cdot \frac{(1 + \beta_{0,1})^2}{\beta_{0,1}}. \quad (37)$$

Since $p_1 \in \mathbb{R}$, equation (37) requires

$$\frac{(1 + \beta_{0,1})^2}{\beta_{0,1}} \in \mathbb{R} \quad \implies \quad \frac{(1 + \beta_{0,1})^2}{\beta_{0,1}} = \frac{(1 + \bar{\beta}_{0,1})^2}{\bar{\beta}_{0,1}}, \quad (38)$$

where the overbar indicates complex conjugation. Solving (38), we find two possibilities: $\beta_{0,1} \in \mathbb{R} \setminus \{0\}$ or $|\beta_{0,1}| = 1$. We exclude the first possibility, as then λ_2 would be imaginary by (36). Hence,

$$\beta_{0,1} = \exp(i\theta), \quad \text{for } \theta \in [0, 2\pi),$$

and equations (36) and (37) become

$$\lambda_2 = \pm i\tilde{c}_g(1)r_1\sqrt{2\Delta_{\text{BF}}} \cos\left(\frac{\theta}{2}\right) + U \sin(\theta), \quad (39)$$

$$p_1^2 = 2\Delta_{\text{BF}} \cos^2\left(\frac{\theta}{2}\right), \quad (40)$$

respectively, where

$$\Delta_{\text{BF}} = -\frac{U}{V} = 2 \left(\frac{\frac{1}{\omega'(0) - \omega'(1)} + \frac{1}{\omega(2) - 2c_0}}{\omega''(1)} \right). \quad (41)$$

In order for $p_1 \in \mathbb{R}$ for any θ , we must have

$$\Delta_{\text{BF}} > 0, \quad (42)$$

which is a sufficient condition for the development of the Benjamin-Feir instability. This condition is equivalent to those derived rigorously in [20, 24–26].

Assuming $\Delta_{\text{BF}} > 0$, equation (40) immediately implies

$$-\sqrt{2\Delta_{\text{BF}}} \leq p_1 \leq \sqrt{2\Delta_{\text{BF}}}, \quad (43)$$

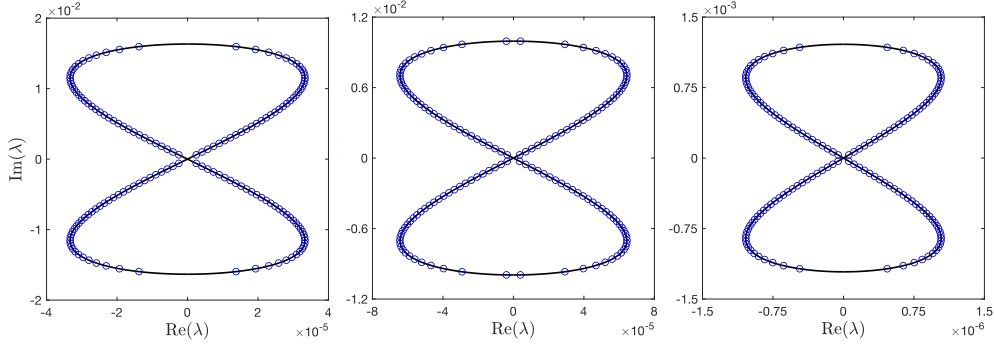


Fig. 6 *Left:* Figure-eight curve for the Kawahara equation with $a = -3$, $b = 1$, and $\varepsilon = 10^{-2}$. The blue circles are computed using the Floquet-Fourier-Hill method; the black curves are the lemniscates predicted by (44). *Center:* The same as the left plot but for the Whitham equation with $h = 2$. *Right:* The same as the left plot but for the capillary-Whitham equation with $h = 2$ and $\sigma = 3$.

so that p_1 is constrained to a real-valued interval that is symmetric about zero, as promised. The eigenvalues corresponding to these Floquet exponents lie on a closed curve of the form

$$\text{Im}\lambda = \pm\varepsilon\tilde{c}_g(1)\sqrt{2\Delta_{\text{BF}}}\cos\left(\frac{\theta}{2}\right)\left(1+r_1\varepsilon\right)+\mathcal{O}(\varepsilon^3), \quad (44a)$$

$$\text{Re}\lambda = \varepsilon^2U\Delta_{\text{BF}}\sin(\theta)+\mathcal{O}(\varepsilon^3). \quad (44b)$$

Truncating this parameterization after $\mathcal{O}(\varepsilon^2)$ and eliminating θ from the real and imaginary parts yields an equation for a lemniscate that approximates the figure-eight curve of Benjamin-Feir eigenvalues. Figure 6 compares this lemniscate to eigenvalues computed numerically using the Floquet-Fourier-Hill method for the Kawahara, Whitham, and capillary-Whitham equations. Excellent agreement is found between the two computations of the eigenvalues, giving confidence in the correctness of our perturbation method.

Remark 4.1. The parameter r_1 is still unknown at this order. Hence, there is remaining ambiguity in the imaginary component of the approximate lemniscate for the Benjamin-Feir eigenvalues. This ambiguity is resolved at the next order. In particular, at $\mathcal{O}(\varepsilon^3)$, the eigenvalue corrections are singular as $\theta \rightarrow 0$ and $\theta \rightarrow 2\pi$. The parameter r_1 is chosen to eliminate this singular behavior so that the third-order corrections to the Benjamin-Feir eigenvalues remain bounded for all θ . This principle is known as the *regular curve condition* and was first introduced in [11–13]. In our case, the regular curve condition yields $r_1 = 0$, similar to the water wave problem in finite depth [14]. In other instances, *e.g.*, the water wave problem in infinite depth, $r_1 \neq 0$, which slightly alters the equation of the approximating lemniscate.

With (44) in hand, we can directly compare the relative strengths of the Benjamin-Feir and high-frequency instabilities *across an entire family of weakly nonlinear dispersive models* for the first time. If the model admits triad high-frequency

instabilities, these instabilities will always dominate the Benjamin-Feir instability at small amplitudes, as the triad instabilities grow as $\mathcal{O}(\varepsilon)$ while Benjamin-Feir grows as $\mathcal{O}(\varepsilon^2)$. In models for which there are no triad instabilities¹, then the Benjamin-Feir instability directly competes with the quartet high-frequency instability. From Section 3.0.3, the most unstable eigenvalue of the quartet instability has leading-order behavior $|-A\sqrt{G/E} + C\sqrt{E/G}|\varepsilon^2$, while that of the Benjamin-Feir instability is $|U\Delta_{BF}|\varepsilon^2$. Thus, for Benjamin-Feir to overtake the quartet instability, one must have

$$\left| -A\sqrt{G/E} + C\sqrt{E/G} \right| < |U\Delta_{BF}|.$$

Otherwise, Benjamin-Feir is subdominant to the quartet high-frequency instability. Should a model have neither triad nor quartet high-frequency instabilities, then Benjamin-Feir dominates at small amplitude by default.

4.1 The Akers–Milewski Equation

From Table 1, the dispersion relation of the Akers–Milewski equation with $\sigma = 1$ is

$$\omega(k) = \text{sgn}(k)(1 + |k|)^2,$$

which violates assumption (iii) in our investigation of the Benjamin-Feir instability. Nevertheless, we can modify our perturbation method to capture the Benjamin-Feir instability in this model as well. To the authors' knowledge, this is the first time that the Benjamin-Feir instability spectrum has been approximated analytically for a model with discontinuous dispersion.

Crucial to the modified perturbation method is a correct expansion of

$$\omega(p + k) = \omega(\varepsilon p_1(1 + r(\varepsilon)) + k),$$

with respect to ε for each $k \in \mathbb{Z}$. By inspection, one sees there are two distinct cases:

$$\omega(p + k) = \begin{cases} \text{sgn}(k)(1 + |\varepsilon p_1(1 + r(\varepsilon)) + k|)^2 & k \in \mathbb{Z} \setminus \{0\} \\ \text{sgn}(\varepsilon p_1)(1 + |\varepsilon p_1(1 + r(\varepsilon))|)^2 & k = 0 \end{cases},$$

where we have used $|\varepsilon| \ll 1$ to simplify the arguments of the sign functions. Both cases can be simplified further if one restricts $\varepsilon > 0$ and uses the identity

$$|s + t| = |s| + \text{sgn}(s)t \quad \text{for } |t| < |s|.$$

Then,

$$\omega(p + k) = \begin{cases} \text{sgn}(k)(1 + \varepsilon|p_1| + \text{sgn}(p_1)r(\varepsilon))^2 & k \in \mathbb{Z} \setminus \{0\} \\ \text{sgn}(p_1)(1 + \varepsilon|p_1| + \text{sgn}(p_1)r(\varepsilon))^2 & k = 0 \end{cases}. \quad (45)$$

¹This would occur when the Krein signature at the corresponding flat-state repeated eigenvalue is non-negative.

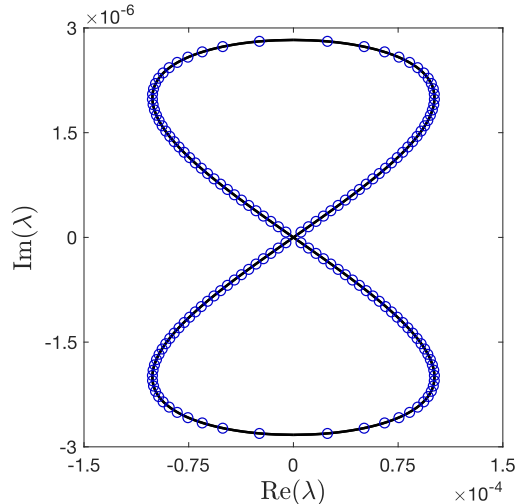


Fig. 7 Figure-eight curve for the Akers–Milewski equation with $\varepsilon = 10^{-2}$ and $\sigma = 1$. The blue circles are computed using the Floquet–Fourier–Hill method; the black curves are the lemniscates predicted by (44).

In both cases, (45) is now a power series in ε , allowing us to proceed formally with the perturbation method.

As a consequence of (45), the $k = 0$ Fourier mode is no longer in the nullspace² of the operator T_0 . Hence, at each order in ε of the perturbation method, there are only two solvability conditions to satisfy, making the computations for the Akers–Milewski equation somewhat simpler. However, one also finds $\tilde{c}_g(1) = 0$ for this model, implying that the imaginary component of the figure-eight curve vanishes at first and second order in ε . Therefore, to get the leading-order lemniscate for the Akers–Milewski equation, one needs to carry out the perturbation method to $\mathcal{O}(\varepsilon^3)$. Working through the calculations, one indeed finds a lemniscate with $\mathcal{O}(\varepsilon^2)$ real component and $\mathcal{O}(\varepsilon^3)$ imaginary component. Figure 7 compares this leading-order lemniscate with eigenvalues computed numerically by the Floquet–Fourier–Hill method, to excellent agreement.

5 Conclusion

We have developed a unified perturbation framework for the spectral stability of small-amplitude Stokes waves in weakly nonlinear model equations of the form (1). By expanding the eigenvalues, eigenfunctions, and Floquet exponent in the wave amplitude and treating the ratio β of the colliding flat-state eigenmodes as a free parameter, we organised the unstable spectrum into sheets of spectral data in $(\text{Re}\lambda, \text{Im}\lambda, p)$ -space.

²Thus, the geometric multiplicity of the zero eigenvalue drops from three to two for the Akers–Milewski equation, but the algebraic multiplicity remains equal to four.

For each fixed β the solvability conditions determine the eigenvalue and Floquet corrections, and varying β traverses the full sheet associated with a given collision. Slices of these sheets at fixed amplitude produce the isolas of instability discussed in [10–13].

For non-zero Floquet collisions, we derived explicit asymptotics for triad and quartet high-frequency instabilities. Triad resonances lead to elliptical isolas of order $\mathcal{O}(\varepsilon)$ centred at the flat-state spectrum, whereas quartet resonances produce $\mathcal{O}(\varepsilon^2)$ isolas whose centres drift along the imaginary axis and whose semi-major axes also scale like $\mathcal{O}(\varepsilon^2)$. Higher-order resonances do not generate instability at these orders. At the triple collision at the origin, we recovered the Benjamin–Feir (modulational) instability, obtained a lemniscate approximation to the figure-eight spectrum, and formulated the perturbation scheme so that it remains valid even when $\omega'(k)$ has jump discontinuities. In particular, we derived, to our knowledge, the first analytic approximation of the Benjamin–Feir spectrum for the Akers–Milewski equation, showing that the method extends beyond smooth-dispersion models.

Because the same framework treats both high-frequency and Benjamin–Feir instabilities across our family of models, it enables a direct comparison of their growth rates in a common setting. When triad instabilities are present, their $\mathcal{O}(\varepsilon)$ growth rates dominate the $\mathcal{O}(\varepsilon^2)$ Benjamin–Feir growth; in the absence of triads, the competition between quartet and Benjamin–Feir instabilities is governed by the model-dependent coefficients appearing in their respective asymptotics. If a model admits neither triad nor quartet high-frequency instabilities, the Benjamin–Feir mechanism becomes the leading small-amplitude source of spectral instability.

Throughout, asymptotic predictions were validated against numerical spectra computed using the Floquet–Fourier–Hill method and a quasi-Newton continuation scheme, with asymptotically correct agreement and examples that highlight the influence of higher-order corrections. The bifurcation structure revealed here is expected to inform future rigorous existence results for unstable spectra and to guide further studies of nonlinear dynamics near the onset of instability in dispersive wave models.

Disclaimer: This report was prepared as an account of work sponsored by an agency of the United States Government. Neither the United States Government nor any agency thereof, nor any of their employees, make any warranty, express or implied, or assumes any legal liability or responsibility for the accuracy, completeness, or usefulness of any information, apparatus, product, or process disclosed, or represents that its use would not infringe privately owned rights. Reference herein to any specific commercial product, process, or service by trade name, trademark, manufacturer, or otherwise does not necessarily constitute or imply its endorsement, recommendation, or favoring by the United States Government or any agency thereof. The views and opinions of authors expressed herein do not necessarily state or reflect those of the United States Government or any agency thereof.

Declarations: B. Akers was supported in part by the Air Force Office of Scientific Research (AFOSR) and the Joint Directed Energy Transition Office (DE-JTO) during the preparation of this manuscript. R. Creedon acknowledges support from the National Science Foundation, grant number NSF-DMS-2402044.

References

- [1] Craik, A.D.: George Gabriel Stokes on water wave theory. *Annu. Rev. Fluid Mech.* **37**(1), 23–42 (2005)
- [2] Benney, D., Roskes, G.: Wave instabilities. *Studies in Applied Mathematics* **48**(4), 377–385 (1969)
- [3] Zakharov, V.E.: Stability of periodic waves of finite amplitude on the surface of a deep fluid. *Journal of Applied Mechanics and Technical Physics* **9**(2), 190–194 (1968)
- [4] Phillips, O.M.: Theoretical and experimental studies of gravity wave interactions. *Proceedings of the Royal Society of London. Series A. Mathematical and Physical Sciences* **299**(1456), 104–119 (1967)
- [5] Benjamin, T.B., Feir, J.E.: The disintegration of wave trains on deep water part 1. theory. *Journal of Fluid Mechanics* **27**(3), 417–430 (1967)
- [6] Dysthe, K.B.: Note on a modification to the nonlinear schrödinger equation for application to deep water waves. *Proceedings of the Royal Society of London. A. Mathematical and Physical Sciences* **369**(1736), 105–114 (1979)
- [7] Davey, A., Stewartson, K.: On three-dimensional packets of surface waves. *Proceedings of the Royal Society of London. A. Mathematical and Physical Sciences* **338**(1613), 101–110 (1974)
- [8] Segur, H., Henderson, D., Carter, J., Hammack, J., Li, C.-M., Pheiff, D., Socha, K.: Stabilizing the benjamin–feir instability. *Journal of Fluid Mechanics* **539**, 229–271 (2005)
- [9] Kapitula, T., Promislow, K.: *Spectral and Dynamical Stability of Nonlinear Waves*. Applied Mathematical Sciences, vol. 185. Springer, New York, NY (2013). <https://doi.org/10.1007/978-1-4614-6995-7>
- [10] Akers, B.F.: Modulational instabilities of periodic traveling waves in deep water. *Physica D: Nonlinear Phenomena* **300**, 26–33 (2015)
- [11] Creedon, R., Deconinck, B., Trichtchenko, O.: High-frequency instabilities of the Kawahara equation: a perturbative approach. *SIAM Journal on Applied Dynamical Systems* **20**(3), 1571–1595 (2021)
- [12] Creedon, R., Deconinck, B., Trichtchenko, O.: High-frequency instabilities of a Boussinesq–Whitham system: a perturbative approach. *Fluids* **6**(4), 136 (2021)
- [13] Creedon, R.P., Deconinck, B., Trichtchenko, O.: High-frequency instabilities of Stokes waves. *Journal of Fluid Mechanics* **937**, 24 (2022)

- [14] Creedon, R.P., Deconinck, B.: A high-order asymptotic analysis of the Benjamin–Feir instability spectrum in arbitrary depth. *Journal of Fluid Mechanics* **956**, 29 (2023)
- [15] Akers, B., Nicholls, D.P.: Wilton ripples in weakly nonlinear dispersive models of water waves: Existence and analyticity of solution branches. *Water Waves* **3**(1), 25–47 (2021)
- [16] Creedon, R.: Existence of all Wilton ripple solutions of the Kawahara equation. arXiv:2411.13508 (2024)
- [17] Deconinck, B., Trichtchenko, O.: High-frequency instabilities of small-amplitude solutions of hamiltonian pdes. *Discrete and Continuous Dynamical Systems* **37**, 1323–1358 (2017)
- [18] Deconinck, B., Kutz, J.N.: Computing spectra of linear operators using the floquet–fourier–hill method. *Journal of Computational Physics* **219**(1), 296–321 (2006)
- [19] Claassen, K.M., Johnson, M.A.: Numerical bifurcation and spectral stability of wavetrains in bidirectional whitham models. *Studies in Applied Mathematics* **141**(2), 205–246 (2018)
- [20] Maspero, A., Radakovic, A.M.: Full description of Benjamin-Feir instability for generalized Korteweg-de Vries equations. arXiv preprint arXiv:2404.06172 (2024)
- [21] Craik, A.D.D.: *Wave Interactions and Fluid Flows*. Cambridge University Press, Cambridge (1988)
- [22] Hammack, J.L., Henderson, D.M.: Resonant interactions among surface water waves. *Annual Review of Fluid Mechanics* **25**(Volume 25, 1993), 55–97 (1993) <https://doi.org/10.1146/annurev.fl.25.010193.000415>
- [23] Nicholls, D.P.: Spectral stability of traveling water waves: Analytic dependence of the spectrum. *Journal of nonlinear science* **17**, 369–397 (2007)
- [24] Bronski, J.C., Hur, V.M., Johnson, M.A.: Modulational instability in equations of KdV type. *New approaches to nonlinear waves*, 83–133 (2016)
- [25] Hur, V.M., Johnson, M.A.: Modulational instability in the Whitham equation for water waves. *Studies in Applied Mathematics* **134**(1), 120–143 (2015)
- [26] Hur, V.M., Johnson, M.A.: Modulational instability in the Whitham equation with surface tension and vorticity. *Nonlinear Analysis: Theory, Methods & Applications* **129**, 104–118 (2015)